Neurotoxicology 77 (2020) 181–192

Contents lists available at ScienceDirect

Neurotoxicology

journal homepage: www.elsevier.com/locate/neuro

Full Length Article

Microglial activation and responses to vasculature that result from an acute LPS exposure

John F. Bowyer[a], Sumit Sarkar[a,*], Susan M. Burks[a], Jade N. Hess[a], Serena Tolani[a], James P. O'Callaghan[b], Joseph P. Hanig[c]

[a] Division of Neurotoxicology, National Center for Toxicology/ FDA, Jefferson, AR 72079, USA
[b] Health Effects Laboratory Division, Centers for Disease Control and Prevention, National Institute for Occupational Safety and Health Morgantown, WV 26505, USA
[c] Center for Drug Evaluation and Research/ FDA Silver Spring, MD 20993, USA

ARTICLE INFO

Keywords:
Lipopolysaccharide
Endothelial cells
Neuroinflammation
Microglia
Blood-brain barrier

ABSTRACT

Bacterial cell wall endotoxins, i.e. lipopolysaccharides (LPS), are some of the original compounds shown to evoke the classic signs of systemic inflammation/innate immune response and neuroinflammation. The term neuroinflammation often is used to infer the elaboration of proinflammatory mediators by microglia elicited by neuronal targeted activity. However, it also is possible that the microglia are responding to vasculature through several signaling mechanisms. Microglial activation relative to the vasculature in the hippocampus and parietal cortex was determined after an acute exposure of a single subcutaneous injection of 2 mg/kg LPS. Antibodies to allograft inflammatory factor (Aif1, a.k.a. Iba1) were used to track and quantify morphological changes in microglia. Immunostaining of platelet/endothelial cell adhesion molecule 1 (Pecam1, a.k.a. Cd31) was used to visualize vasculature in the forebrain and glial acidic fibrillary protein (GFAP) to visualize astrocytes. Neuroinflammation and other aspects of neurotoxicity were evaluated histologically at 3 h, 6 h, 12 h, 24 h, 3 d and 14 d following LPS exposure. LPS did not cause neurodegeneration as determined by Fluoro Jade C labeling. Also, there were no signs of mouse IgG leakage from brain vasculature due to LPS. Some changes in microglia size occurred at 6 h, but by 12 h microglial activation had begun with the combined soma and proximal processes size increasing significantly (1.5-fold). At 24 h, almost all the microglia soma and proximal processes in the hippocampus, parietal cortex, and thalamus were closely associated with the vasculature and had increased almost 2.0-fold in size. In many areas where microglia were juxtaposed to vasculature, astrocytic endfeet appeared to be displaced. The microglial activation had subsided slightly by 3 d with microglial size 1.6-fold that of control. We hypothesize that acute LPS activation can result in vascular mediated microglial responses through several mechanisms: 1) binding to Cd14 and Tlr4 receptors on microglia processes residing on vasculature; 2) damaging vasculature and causing the release of cytokines; and 3) possibly astrocytic endfeet damage resulting in cytokine release. These acute responses may serve as an adaptive mechanism to exposure to circulating LPS where the microglia surround the vasculature. This could further prevent the pathogen(s) circulating in blood from entering the brain. However, diverting microglial interactions away from synaptic remodeling and other types of microglial interactions with neurons may have adverse effects on neuronal function.

1. Introduction

Lipopolysaccharides (LPS) are bacterial cell wall endotoxins known to evoke the classic signs of systemic inflammation and neuroinflammation in the brain (Buchanan et al., 2010; Catorce and Gevorkian, 2016; Laflamme et al., 2001; Lopes, 2016; Rosadini and Kagan, 2017). These effects are characterized by the elaboration of proinflammatory mediators from the systemic immune system or neuroimmune system. These effects can be viewed as restorative and physiological, in the case of the induction of sickness behavior, but also can have significant adverse neurological effects (Dantzer et al., 2008). The importance of these effects is highlighted by the fact that induction of either the

Abbreviations: Aif1 a.k.a Iba1, allograft inflammatory factor 1; BBB, blood-brain barrier; Cd14, CD14 molecule; DAB, diaminobenzedine; FITC, fluorescein isothiocyanate; FJc, Fluoro-Jade C; GFAP, glial fibrillary acidic protein; METH, methamphetamine; a.k.a Cd31, Pecam1; TRITC, tetramethylrhodamine-isothiocyanate; Tlr4, toll-like receptor 4

* Corresponding author at: National Center for Toxicological Research/FDA, 3900 NCTR Road, HFT-132, Jefferson, AR-72079, USA.
E-mail address: Sumit.Sarkar@fda.hhs.gov (S. Sarkar).

https://doi.org/10.1016/j.neuro.2020.01.014
Received 13 August 2019; Received in revised form 29 January 2020; Accepted 31 January 2020
Available online 31 January 2020
0161-813X/

systemic immune system or the neuroimmune system can have significant adverse mental effects (Dantzer et al., 2008). A possible cause of these adverse effects on mental function may be related to diverting microglia activity away from their role in neuronal function and towards vasculature interactions. A loss of microglial interactions involved in forming synapses and remodeling synapses can lead to mental dysfunction, which is a process that plays a role in several mental illness classifications and cognitive function deficits (Aldskogius et al., 1999; Bisht et al., 2018; Bruce-Keller, 1999; Graeber, 2010; Graeber and Streit, 2010; Kraft and Harry, 2011; Lenz and Nelson, 2018; Savage et al., 2018; Tremblay, 2011).

Previous research from our laboratories on the role of microglia in acute neurotoxic insults have indicated that microglia activation is in response to neurodegeneration and vascular damage and not the cause of it (Bowyer et al., 2016, 2018a; Kelly et al., 2012; O'Callaghan et al., 2008). As well, gene expression at the protein and mRNA level indicates that an acute LPS exposure 14 days or less does not result in neurodegeneration. However, LPS may have other effects that are detrimental to brain function (Kelly et al., 2012, 2018; O'Callaghan et al., 2008, 2015). These effects are in line with views of other investigators (Graeber and Streit, 2010; Streit, 2010), that microglia activation seldom, if ever, initiates neurodegenerative processes and that activation is often beneficial to neuronal function. Nevertheless, diversion of microglial activity away from neuronal processes and towards their roles in maintaining vascular function and protecting against infection could have detrimental neurological effects.

Many investigators have ascribed LPS activation of microglia as a source of the subsequent neuroinflammatory cytokines or chemokines elicited from neuronal populations and/or perhaps the astrocytic population. A more direct mechanism for microglial activation would be through interactions with LPS on CD14 molecules (Cd14), Toll-like receptors (Tlr4) present on microglia (Hoogland et al., 2015), and the NLRP3 inflammasome complex. However, LPS is known to damage the integrity of the endothelium of the gut, liver and, even more pertinent, the lung vasculature, by disrupting their tight junctions (see reviews (Guerville and Boudry, 2016; Kasa et al., 2015)). Again, these LPS responses likely are mediated by Toll-like receptor pathways (Khakpour et al., 2015).

Thus, we hypothesize that brain vasculature would be adversely affected by LPS and this would /will lead to microglial activation in response to this damage. It would also not be surprising if LPS had some adverse effects on vascular endothelium of the brain, and that this effect may be in some way contributing to the microglial activation and "neuroimmune" response seen in the brain. Indeed, vascular disruption and leakage produced by methamphetamine (METH) can evoke microglia activation which is directed toward brain vasculature (Bowyer et al., 2016). Also, microglia activation due to thiamine deficiency, which affects vascular integrity, appears directed toward brain vasculature in the thalamus (Bowyer et al., 2018b).

The main objective of the present study was to determine the time course of microglial activation after a single LPS exposure, and to determine the potential for LPS to alter the spacial distribution of the activated microglia with respect to vasculature. Allograft inflammatory factor (*Aif1*; a.k.a Iba1) immunoreactivity was used to track microglial morphological changes and its association with vasculature and astrocytes (Imai et al., 1996; Ito et al., 1998). Glial fibrillary acidic protein (GFAP) and platelet and endothelial cell adhesion molecule 1 (*Pecam1*; a.k.a Cd31) immunoreactivity were used to identify astrocytes and vascular endothelium, respectively. Increased mouse IgG and albumin immunoreactivity was used to histologically identify and localize extravascular IgG to enable the detection of blood-brain barrier (BBB) leakage/disruption. The female BALB/C mouse was chosen since its vasculature is responsive to insults that can disrupt the blood-brain barrier (On et al., 2013; Xaio et al., 2001) and has been used to observe vascular-directed microglial responses during the development of thiamine deficiency neurotoxicity (Bowyer et al., 2018b).

2. Materials and methods

2.1. Animals

This study was carried out in accordance with the Guide for the Care and Use of Laboratory Animals as adopted and promulgated by the National Institutes of Health. The use of animal testing in this study was done under protocols E7579 (issued to John Bowyer) that were approved by the NCTR institutional animal care and use committee (IACUC), which is fully accredited (Food and Drug Administration - National Center for Toxicological Research Accreditation #A4310-01) by NIH-OLAW. Fifty female BALBc mice (70 ± 5 days old, 19 ± 2 g) were obtained from Jackson Laboratories (JAX). Animals were tattooed with ink in the tail for identification and then held until they were 85–90 days of age before initiation of testing. Animals were housed four/cage in the NCTR facility in isolator top boxes with wooden chip bedding and food and water ad libitum. The light cycle of the animal room was maintained under a 12/12 h (6 am-6 pm lights on) schedule. Animals were randomly selected for dosing (saline versus LPS) and time of sacrifice, but with littermates equally separated into different treatment groups and sacrifice times as much as possible. The average weight of each dosing group was not significantly different.

2.2. Study design

The treatments groups consisted of a control groups given a single injection of 2 ml/kg normal saline and the LPS groups, which were all given a single injection of 2 mg/kg LPS s.c. in a 2 ml/kg volume. There were multiple sacrifice time points for the LPS treatment at: 3 h (n = 5); 6 h (n = 6); 12 h (n = 6); 24 h (n = 6); 2 d (n = 3); 3 d (n = 6) and 2 weeks (n = 4). There were two saline control groups with one sacrificed at 3 h (n = 5) and one after 24 h (n = 7). All dosing occurred between 7:30 am and 9:00 am. There were only two control groups because we have previously observed no overall significant differences in the distribution of microglial sizes in adult female BALBc controls in our previous experiments (Bowyer et al., 2018b). Animal behavior was monitored every 15 min for the first 4 h after saline or LPS and every 1 h thereafter. Body temperature was monitored every 2 h for the first 12 h using a T-type mouse rectal probe (RET-3) coupled to a BAT-10 thermometer from Physitemp Instruments Inc. (Clifton, NJ, USA) inserted rectally to a length of 2 cm into the colon.

All groups except the 3 h saline and LPS groups, were composed of mice generated in three replicate experiments conducted over a 1.2-year period. Each replicate contained two LPS mice at each of the time points and 2 or 3 saline controls. These animals were formalin perfused for determining level of microglial activation and microglial location relative to vasculature and astrocytes. The data from the controls at 3 h and 2 mg/kg LPS at 3 h was generated after the previous three replicates. These animals were specifically used to histologically determine whether IgG leakage/extravasation had occurred. These two groups were perfused with 30 ml saline and then the brain was split in half. One hemisphere was postfixed in formalin for use for the data reported herein while the other was used to determine mRNA levels in cortex and hippocampus (to be used to generate data for a subsequent publication).

2.3. Animal sacrifice and preparation for histological analysis

The perfusion procedure necessary for histological processing was initiated by giving a lethal dose of approximately 150 to 300 mg/kg i.p. of pentobarbital and 20–40 mg/kg sodium phenytoin (0.25 to 0.5 ml of Euthasol® from Vibrac AH, Inc. containing in 390 mg/ml pentobarbital and 50 mg/ml sodium phenytoin). Mice were sacrificed between 11:00 am and 8:00 pm. When the respiration was barely detectable and there was no response to either tail or foot pinch (pain), mice were perfused with 15–20 ml of saline followed by 35–50 ml of 4 % formaldehyde in

0.1 M sodium phosphate buffer (pH 7.4). Details of the perfusion procedure have been previously reported (Bowyer et al., 1998).

Brains were postfixed for 24–36 h in 4 % formaldehyde in 0.1 M sodium phosphate buffer pH 7.4 (NaPB) and then transferred to a 20 % sucrose in 0.1 M sodium phosphate buffer solution for 1 d to 2 d. The forebrains were then blocked removing the cerebellum and snap frozen by placing them on an aluminum plate resting on dry ice and smothering the brain with finely crushed dry ice. Sectioning of the brain was performed using a cryostat. Prior to sectioning, the forebrains were embedded in OCT compound (Electron Microscope Science, Hatfield, PA, USA) and mounted on a Leica Cryostat for cutting coronal sections 25 μm thick from +1.2 to -6.0 relative to the Bregma (Paxinos and Watson, 1995). All brain sections were collected in sodium phosphate buffer containing 0.08 % sodium azide.

2.4. Histochemical and immunohistological labeling

2.4.1. Iba1, albumin and IgG immunohistochemistry

Coronal sections from the parietal cortex (0.4 to -0.4 from bregma), hippocampus and thalamus (-2.8 to -3.5) were used for immunohistochemical processing. Free-floating sections agitated on an orbital shaker were used for immuno-reactive labeling of brain sections with antibody to Iba1 (a.k.a, allograft inflammatory factor 1 (Aif1)) with DAB visualization (shown in Figs. 1 and 2). Sections were first washed 15 min in 0.1 M NaPB in double deionized water and then incubated in 0.1 M NaPB containing 0.3 % H_2O_2 for 30 min to destroy the endogenous peroxidases. From this point on, except with the last step of DAB processing, the incubation and washing solutions consisted of NaPB containing 0.4 % Triton X-100. Subsequently, sections were washed 3X for 5 min per wash. After a 30 min pre-incubation in 4 % normal goat serum, the sections were incubated in serum and rabbit anti-Iba1 (1:1000 dilution, Wako Inc., Japan) antibody for 1–2 h followed 18–24 h at 5 °C. Sections were then washed 3X for 10 min and incubated in a goat anti-rabbit antibody (1:200; Vector Laboratories, Burlingame, CA) for 1–2 h. The signal was amplified using the avidin and biotinylated horseradish peroxidase macromolecular complex (ABC, Vector Laboratories) and visualized with 0.4 mg/ml of 3,3′-diaminobenzidine (DAB) in 0.1 M NaPB buffer. Sections were then washed 2X (5 min per wash) in NaPB and mounted on slides. Finally, the slides were cleared in xylene and cover-slipped with DPX mounting medium.

Similar methods enabled localization of mouse IgG with a biotinylated goat anti-mouse IgG antibody (1:200; Vector Lab. Inc., Burlingame, CA) followed by the ABC complex method and subsequent visualization of DAB as previously described. The same methods were used for DAB immune-localization of albumin using polyclonal primary antibody (Proteintech). Mouse IgG was localized using a goat biotinylated primary antibody to mouse IgG (Vector Laboratory Inc., Burlingame CA)) directly followed by the ABC method with subsequent DAB visualization.

2.4.2. Combined Cd31 or Aquaporin 4 with Iba1 immuno-localization

Co-visualization of vasculature with microglia, as shown in Fig. 3, was performed by using antibody to Cd31 and DAB for visualization and subsequently immune-localization of Iba1 immunofluorescence method. Following incubation with 0.3 % H_2O_2 for 30 min, the sections were washed 3 × 5 min in 0.4 % Triton X-100 buffer (this buffer was used as the medium for the remaining incubations excepting the DAB visualization step). Sections were incubated in 4 % goat serum for 30 min and then incubated (2 h room temperature then overnight at 4 °C) in a purified rat anti-mouse antibody (1:500; BD Pharmagen) to Cd31. The sections were washed 3 × 5 min followed by incubations in a biotinylated goat anti-rat secondary antibody combined with ABC reactions followed and finally DAB visualization (same methods previously described above for Iba1).

Following Cd31 & DAB labeling, the sections were washed 3X (15 min per wash) in NaPB containing 0.4 % Triton X-100. Sections were then washed in PBS and pre-incubated with 5 % goat serum (GIBCO, USA) made in PBS for 20 min and then incubated with rabbit polyclonal antibody to Iba1 primary antibody (1:500; Wako) for 24 − 48 h at 4C°C. After 48 h, tissue sections were rinsed in PBS containing Triton-X for 3 − 5 min 3X followed by incubation in biotinylated secondary antibody (1:200) for 2 − 3 h at RT using PBS as antibody diluent. Then sections were washed in PBS containing Triton-X for 3 − 5 min and incubated in Streptavidin TRITC (Jackson Immunoresearch, PA, USA) for 2 h are RT. Then tissue sections were rinsed in PBS containing Triton-X for 3 − 5 min for 3 × . Subsequently, sections were mounted in distilled water containing 0.1 M PB, dried in a warmer and cleared in xylene and coverslipped in DPX mounting medium and dried overnight under the hood.

For dual fluorescent labeling, a cocktail of primary antibodies was used for simultaneously labeling the vasculature with mouse anti-rat aquaporin 4 primary antibody (1: 200; Abcam) and an Iba1 antibody (1:500, Wako Inc) for labeling the microglia. Subsequently, sections were incubated for 2 h in secondary goat anti-rabbit (1:200; Jackson Immunoresearch) antibody for aquaporin4 localization. Finally, the sections were incubated in a cocktail containing Streptavidin-TRITC (1:200; Jackson Immunoresearch) for Aquaporin 4 and Alexa Flour 488 Chicken anti-Rabbit IgG (1:100; Thermofisher scientific) for IBA1 localization for 2 − 3 h. Sections were then mounted as previously described.

2.4.3. Combined Iba1 and DAPI immuno-localization for nuclei and microglia overlap

Free floating sections were incubated with 0.3 % H_2O_2 for 30 min, the sections were washed 3 × 5 min in 0.4 % Triton X-100 buffer (this buffer was used as the medium for the remaining incubations excepting the DAB visualization step). Succeeding methods for Iba1-TRITC labeling were the same as those described above for the Cd31 and Iba1 co-labeling. Iba1-TRITC labeled sections were washed and mounted on slides as described above. They were then coverslipped using Fluoroshield™ with DAPI (4′,6-diamidino-2-phenylindole) mounting medium and dried overnight under the hood.

2.4.4. Combined Cd31, GFAP and Iba1 immunohistochemistry

Co-localization of vasculature, microglia and astrocytes was accomplished by first immunolabeling the vasculature with DAB and an antibody to CD31 as previously described above. After DAB visualization, the sections were washed 3 × 15 min in 0.4 % Triton X-100 buffer (this buffer was used as the medium for the remaining incubations and washes). The sections were then incubated in 5 % goat serum for 20 min at RT; subsequently, sections were incubated in a cocktail of chicken anti GFAP (1:500; Thermofisher scientific, USA) and polyclonal Rabbit IBA1 (Wako, Japan) for 48 h at 4 °C. After 48 h of incubation, sections were incubated in biotinylated goat anti chicken secondary IgG (1:200; Novex, USA) at RT for 2 h. Sections were then washed in PBS and Triton X-100 for 2–3 times. Then, sections were incubated in a cocktail of FITC-streptavidin (1:250; Vector Laboratories; CA, USA) and goat anti Rabbit Cy5 secondary IgG (1:150; Vector Laboratories; CA, USA). In this immunolabeling method green fluorescence denotes GFAP containing astrocytes and red fluorescence denotes IBA1 containing microglia.

2.4.5. Fluoro-Jade C labeling

Methods similar to Schmued et al. (Schmued et al., 2005) were used to detect degenerating neurons, dendrites, axons and terminals in the forebrain using Fluoro-Jade C (FJc). Briefly, sections were mounted on gelatin (Sigma, 300Bloom)-coated slides and dried at 50 °C. They were then transferred sequentially through solutions of 100 % ethanol (8 min), 95 % ethanol (2 min), 70 % ethanol (2 min), and 2X double deionized water (2 min). They were then immersed in double distilled water containing 0.06 % potassium permanganate for 8–10 min followed by 2X double deionized water wash (2 min). Labeling was

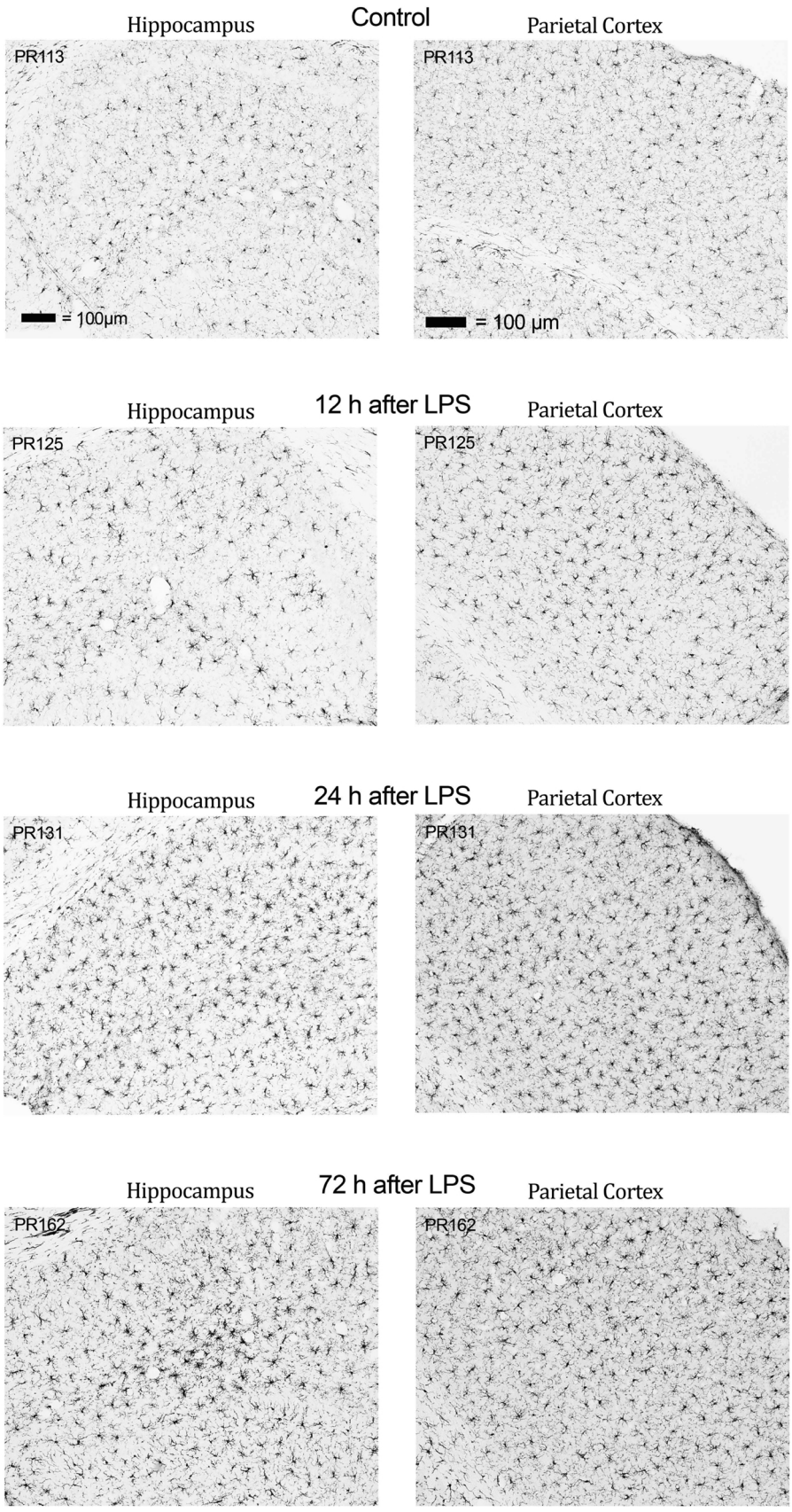

Fig. 1. Progression of the LPS-mediated microglial activation in the hippocampus and parietal cortex. Microglia that are Iba1-DAB immunolabeled/reactive are shown in the CA1 regions of the dorsal hippocampus and parietal cortex in control and at 12 h, 24 h, and 72 h after LPS administration. Representative panels from control or the time points after LPS exposure are shown. It is apparent that activation has started by 12 h, and by 24 h activation is pronounced and occurring in most microglia present. Magnification is the same for all panels and is present in the control micrograph shown in the top two panels.

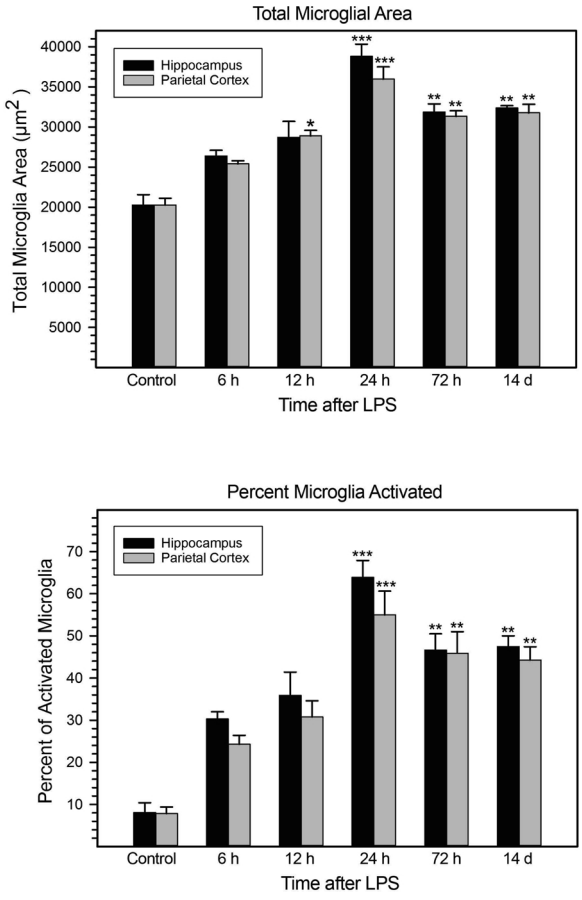

Fig. 2. Progression of increase microglial size and total microglia area within the hippocampus and parietal cortex. Increases in the total area of microglia and (top graph) microglia deemed to be likely activated (bottom graph) within a portion of the selected dorsal CA1 region and parietal cortex are shown at 6 h,12 h, 24 h, 72 h and two weeks after LPS administration. See the Supplemental File for Fig. 2 to obtain the details of the statistical analysis of the data. The average microglial area shown for a treatment group was calculated as the average ± SEM of the total microglial area (μm^2) for each mouse within the ROIs of hippocampus or parietal cortex. The average ± SEM number of microglia deemed as potentially "activated," those with an area (soma + proximal processes) of ≥ 300 μm^2 within the ROIs of hippocampus or parietal cortex, were also determined for controls and LPS groups. The seven control mice shown were all sacrificed at 24 h with 24 h LPS group. They were not used in the two-way ANOVA but are shown because they can be directly compared to the 24 h post LPS group. * 12 h LPS significantly greater than 6 h LPS at $p < 0.05$. ** 14 day and 72 h groups significantly greater than the 6 h and 12 h LPS groups at $p < 0.05$. *** 24 h LPS significantly greater than all other LPS groups at $p < 0.001$.

performed in a 0.00.1 % FJc (Millipore, USA) in 0.1 % acetic acid and distilled water solution followed by rinsing in double distilled water 3X (1 min per wash) to remove excess label. Slides were then rapidly air dried, xylene-cleared, and coverslipped with DPX (Fluka/Sigma, St. Louis, Mo) mounting media.

2.4.6. Microscopy visualization

Histological evaluation of the slide-mounted tissue was performed using a Nikon epifluorescent microscope 80i (Nikon Instruments Inc., Melville, NY) and an X-Cite 120 LED light source (Excelitas Technologies®, Waltham, MA). The following sets of filters were used for visualizing fluorescent labeling in conjunction with the histochemical or immuno-histological labeling: TRITC labeling of Iba1 was visualized using a TRITC-B filter with an excitation of 543 and an emission of 593; FJc labeling with a FITC filter with an excitation of 464.5–499.5 and an emission of 516–556 nm; nuclei labeled with DAPI with a DAPI filter with an excitation of 361–389 and emission of 430 − 490 nm; Cy5 labeling of Iba1 with a Cy5 filter with an excitation of 663–738 and emission of 590-650. Visualization of all DAB-labeled sections was done with incandescent illumination. The DAB reaction with H_2O_2 for chromogen visualization was from 5 to 8 s in duration in all instances with Cd31-DAB, Iba1-DAB, and IgG-DAB antibody labeling. (The visually observed intensity of the DAB labeling is a good indication of the length of the DAB reaction and/ or the extent of non-specific labeling occurred. These factors enabled reproducible quantifications of microglial size. Adjusting the light intensity or the exposure time during imaging is not a very satisfactory method of correcting for variability in DAB labeling intensity of microglia.) All photomicrographs of the images were taken using a Nikon DS-Ri1 using the NIS Elements software from Nikon.

2.4.7. Quantitation of microglial size/activation in parietal cortex and hippocampus

Methods used for quantifying microglial size were like those previously used with some modifications (Bowyer et al., 2017, 2018b). The Sholl analysis (Sholl, 1956), which is capable of differentiating different types of microglia even in resting or non-activated states, was not needed to detect the large increases in size of microglia due to LPS. The intensity of the stained sections, from visual inspection, used for quantitation were selected so that all the sections for all the animals were close in intensity (darkness) of staining.

All photomicrographs were captured using a 10X lens rather than a 4 × . This was done to capture more of the processes proximal to the soma in control animals. Both hemispheres from three sections were evaluated per animal, and were select at ≅-1.5, ≅-1.8 and ≅-2.1 from the bregma. These micrographs were then processed using the NIS Elements Software (Nikon Instruments Inc., Melville, NY) to detect and measure microglia areas within the analyzed region of interest (ROI). The ROI was standardized and kept constant for all mice. The intensity range selection points for detecting the microglia were set to eliminate (as much as possible) as many of the minor processes not connected to somas (Supplemental File 1). However, many of the darkly stained isolated distal process were still captured. Setting intensity capture parameters to exclude all the darkly stained distal processes was not an option since it resulted in exclusion of smaller or more lightly stained microglia soma and adjoining processes. The sphericity parameter was not utilized during object selection since many of the microglia were not ovate or spheroid in nature. The unconnected distal processes, which were smaller with an area of < 60 μm^2, were removed through data filtering.

Because the activation was so widespread and prominent in magnitude in most of the microglia and at most of the sacrifice time points after LPS, other aspects of analysis were also modified. The sum of all the individual microglial areas within the ROI as well as the number of individual microglia with areas greater than 300 μm^2 (likely to be activated) in each mouse were used to assess activation. In the control mice, there were approximately 100–110 objects in the ROI of both parietal cortex and hippocampus that were determined to be microglia having both a soma and proximal. These 100+ microglia in both the hippocampus and the parietal cortex all had an area of > 60 μm^2 on the captured micrographs containing the ROIs and processed by Nikon NIS elements.

However, in the micrographs of the LPS-treated mice, there were more objects greater than 60 μm^2 per ROI (125–200 ROIs). This increase in number is likely not due to an increased number of microglia within the ROIs but due to many of the microglial processes not having soma within the section, greatly enlarging and becoming greater than 60 μm^2 in area. Thus, to avoid an overestimation of the total microglial area within an ROI, only the 105 objects with the highest area in the ROI were summed to determine the total microglial area in the LPS groups. The total numbers of microglia within an ROI with areas

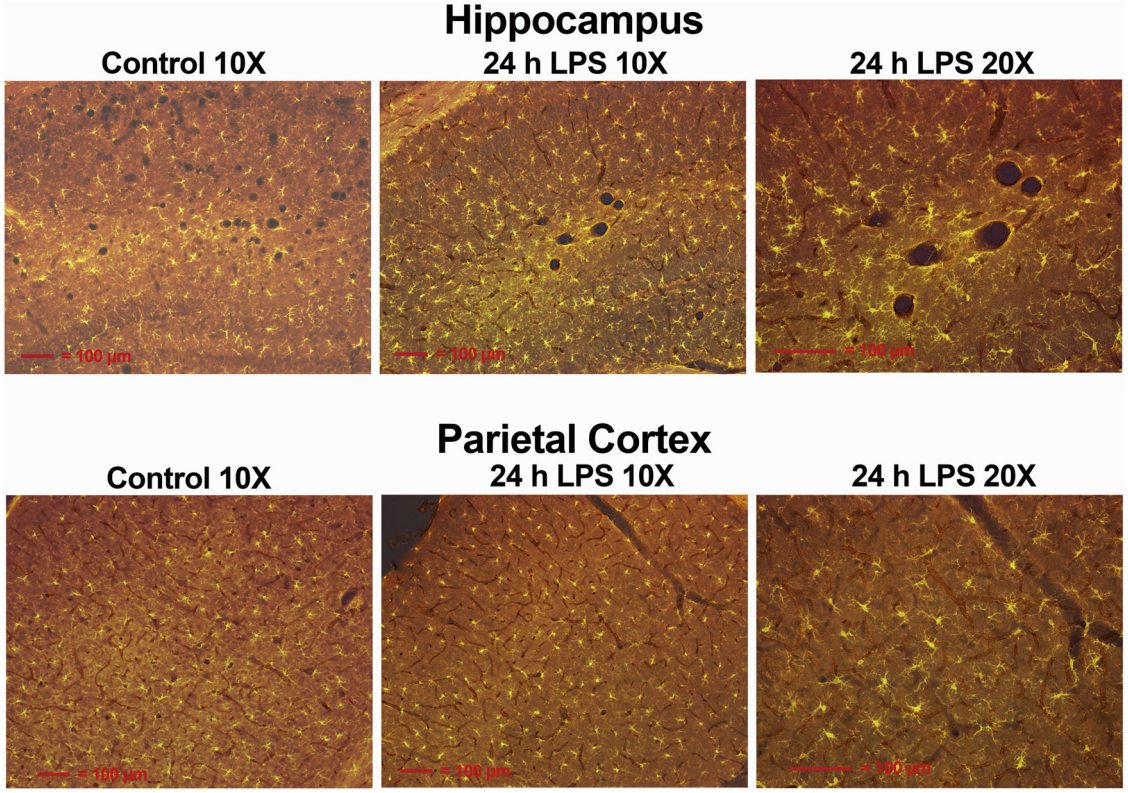

Fig. 3. Activated microglia surrounding the vasculature of the hippocampus and parietal cortex24 h after LPS. Cd31-DAB immunolabeled vasculature (brown) and Iba1- immunolabeled microglia (golden color; TRITC) in controls versus LPS-treated mice are shown. The top panels show LPS effects in the hippocampus at 24 h after exposure compared to control. Most of the microglia are juxtaposed and surrounding the vasculature. The same effect of LPS on microglia at 24 h after exposure can be seen in the parietal cortex in the bottom panels. Again, LPS exposure results in the activated microglia being juxtaposed and surrounding the vasculature. Magnification are shown in the lower left of each panel.

of > 300 μm^2 were also used to evaluate activation since there were few microglia with an area this size in controls.

A two-way ANOVA was used in SigmaPlot to determine whether the changes in total microglial area and number of microglia with an area > 300 μm^2 were dependent on time after LPS administration or brain region. Due to constraints on animal use and the fact that we have observed numbers and sizes of microglia in control animals that are relatively consistent, we only had two control groups. Thus, only the 24 h post LPS group could be directly compared statistically to the 24 h controls.

2.4.8. Quantitation of microglial distances from vasculature and soma size of juxtaposed microglia in hippocampus, parietal cortex and thalamus

In the 24 h group, sections used for co-visualization of vasculature with microglia were imaged at 20 × . Images

were merged in NIS-Elements Advanced Research v5.20.02 (Nikon Instruments Inc., Melville, NY). The distance from the exterior of each soma in the 20x field of view to the exterior of the closest vessel was measured using the distance measurement module. Soma within 1 µm or less of the vasculature were considered "0" for this analysis. Once the distances from all somas to closest vasculature was measured in an image, the average was taken. Number of soma per image ranged from 32 to 64 in the hippocampus, 37–77 in the parietal cortex, and 29–49 in the thalamus. Data were entered into GraphPad Prism 6 (GraphPad Software, San Diego, CA) and a two-way ANOVA used to determine whether the changes in distance showed an effect of treatment and/or region.

Using the same merged images, the number and area of microglia within 1 µm of the vasculature was also determined. The distance measurement module was utilized to measure proximity to vasculature. Somas included were required to measure minimally 5 µm in width, the typical size of a nucleus. Somas were also required to have a difference in intensity of at least 20 from the background. The taxonomy application was then utilized to track the number of somas touching vasculature versus somas greater than 1 µm away in the 20x field of view. Additionally, polygonal ROI were drawn around the somas within 1 µm of vasculature and the ROI statistics utilized to determine the total area (μm^2) occupied by those somas. For proximal processes to be included in the ROI, the width of the cell region had to exceed 1.5 µm.

The number of soma were entered into GraphPad Prism 6 (GraphPad Software, San Diego, CA) and a two-way ANOVA used to determine whether the changes in number of glia within 1 µm showed an effect of treatment and/or region. With a false discovery rate of 6 %, t-tests were also used to determine if the total area of microglia soma within 1 µm of the vasculature was affected by treatment within each region.

3. Results

For the first 4–6 h after LPS the temperature of the mice given LPS dropped 1–2.5 °C compared to control (data not shown). Also, as visually determined, lethargy and decreased locomotor activity were observed after temperature monitoring in the LPS mice for the first 4 h. However, more than 6 h after LPS the behaviors and body temperatures of the LPS-treated mice were not different from controls.

There was no evidence of neurodegeneration as evaluated by FJc labeling in the parietal cortex, hippocampus or thalamus at any of the timepoints evaluated (Supplementary Fig. 2 and 3). As well, there were no obvious increases in IgG (Supplementary Fig. 4 and 5 Fig. 4, Fig. 5) or albumin (data not shown) in the forebrain at either 3 h or 6 h after LPS compared to controls.

A two-way ANOVA was performed using brain region and time after

LPS as the two independent variables and chose either the total microglial area or number of microglia with a size greater than 300 μm^2 as the dependent variable/data (Fig. 2). We used an area of > 300 μm^2 as the criteria for specifying "activation" since in two of the seven control mice the microglia were all less than 300 μm^2. Results showed that there were significant changes in total microglial area and number of microglia with a size greater than 300 μm^2 but no significant differences between the response of the hippocampus and the parietal cortex (only two regions quantified). There was a significantly greater total microglial area present in the mice at 12 h compared to 6 h within the ROI in the parietal cortex (Figs. 1 and 2 and Supplemental File 2). At 24 h post LPS, the total microglia area was seen averaging about 200 % of control with over 50 % of the individual microglia within the ROIs of the hippocampus. The average of the individual total microglial areas was only slightly over 150 % of control at 72 h and with over 40 % of the individual microglia within the ROIs of the hippocampus and the cortex being potentially activated. The microglia in both the cortex and the hippocampus still showed signs of activation at 2 weeks but the sample size was less. Only the 24 h LPS group can be directly compared to the 24 h control group statistically, and both parameters used to monitor activation were significantly greater in LPS group ($p < 0.0001$). The time course of the increase in microglia size is consistent with previous reports of activation/neuroinflammation due to LPS (Kelly et al., 2018).

Only the top 105 microglia with the highest individual areas on the ROI region of the micrographs of the LPS treated mice were summed to determine the total microglial area while in controls all microglia with an area of ≥ 60 μm^2 (resulted in summing the areas from 105 to 120 individual microglia in the seven mice) were used. We determined, via visually counting multiple sections, in previous studies (Bowyer et al., 2017, 2018b) and confirmed in this study (data not shown) that from between 100 and 110 microglia are present in the ROIs used in the two regions. If one was to sum all the microglia with areas ≥ 60 μm^2 in the LPS treated groups, the increase in average total microglial area per mouse-ROI would be about 15–30% greater than shown in Fig. 2 for the 12 h and later time points. We saw no evidence that microglia were replicating and increasing in number and previous experiments using similar doses of LPS in C57BL/6 mice do not show transcriptional changes indicating the microglia are replicating. The additional Iba1-labeled objects (no soma within the section imaged) with areas > 60 μm^2 in the LPS treated groups are likely primarily due to very large proximal process complexes from activated microglia whose soma resided just outside the section being imaged. Supplemental Fig. 6 shows this graphically at 24 h after LPS. The 4′,6-diamidino-2-phenylindole (DAPI) labeled nuclei that overlap (as indicated with red arrows) with Iba1-TRITC labeled microglia produce a whitish region within the soma within the section imaged in Supplemental Fig. 6. However, there are many of the TRITC labeled microglia > 60 μm^2 (as indicated by green arrows) that do not have a DAPI labeled nucleus within them because their soma is not within the imaged section in this Supplemental Figure.

During peak of activation at 24 h, microglia were predominately surrounding the vasculature in the hippocampus and the parietal cortex (shown in Fig. 3) as shown with dual labeling of the vasculature (Cd31-DAB), appearing brownish in color, and the microglia (Iba1-TRITC), appearing golden in color. Not only are the microglia soma larger but become elongated and appear more closely associated with vasculature but also larger and smaller proximal processes are in close vicinity to the vasculature 24 h after LPS. Fig. 4 shows examples of the microscopic images used in both the hippocampus and parietal cortex. The images shown in Fig. 4 are much lighter/brighter than that seen in Fig. 3 because the brightness intensity was increased (via Photoshop) in the Fig. 4 plates. This change in intensity in Fig. 4 can be readily seen in the much lighter appearances of the vascular lumen in Fig. 4 compared to Fig. 3, and it enables a better visual determination of distance of the microglia to the closest vasculature to the reader. The apparent increase in microglia size with fluorescent labeling is quite apparent after LPS like that previously seen with DAB staining methods.

Supplemental Figures 7, 8 and 9 show the visual results in five 24 h controls and six24 h post LPS mice. The association with microglial in the hippocampus, parietal cortex, and thalamus with the same processing used to generate Fig. 4. However, the original (unaltered by PhotoShop) micrographs were analyzed with Nikon NIS Elements to quantify the distances of the microglia from the closest vessel and the microglia soma size for all three brain region (see Methods). These images were used to generate the numerical data in Supplemental File 3 that determined the spatial relationships for all three regions shown in Fig. 5. The top bar graph shows the average distance of all microglia to the nearest vessel in the 20x field of view. In this graph, the microglia in the hippocampus were significantly closer to the vasculature after LPS ($P \leq 0.05$) but not so in the parietal cortex (layers I to IV evaluated) or thalamus. As well, the microglia present in the parietal cortex are much closer than in the hippocampus under control conditions and after LPS ($P \leq 0.001$). The number of microglia within 1 μm of a vessel shown in the middle graph of Fig. 5 indicated a trend towards increasing after LPS, although not significantly different. Percentage wise, these numbers represent approximately 44.5 % (control) and 51 % (LPS) in the hippocampus, 47 % and 49.8 % in the thalamus and 55.9 % and 64.2 % in the parietal cortex, respectively. In all regions, there was no statistical significance using a two-way ANOVA comparing control and 24 h after LPS. The bottom graph in Fig. 5 clearly indicates that the total area of the microglial soma within 1 μm of the closest vessel significantly increases ($P \leq 0.05$). This is likely due to the increase in soma size within 1 μm of the closest vessel after LPS. This also partially due to some of microglia soma within 1 μm to the vasculature elongating.

Triple labeling enabled the visualization (Fig. 6) of the relative positioning of the astrocytes (GFAP immunolabeling with FITC) appearing bright green and microglia (Iba1 immunolabeling with Cy5) appearing red around vasculature (Cd31 immunolabeling with DAB) appearing brownish in color. In this figure the close association of the activated microglia with the astrocytic endfeet on the vasculature can be seen (as indicated by the white arrows) in the hippocampus under control conditions (top panel). In the controls, microglia processes are only seen in a few instances juxtaposed to the vasculature. However, at 24 h after LPS more of the microglia processes appear to be directly in contact with the vasculature (as indicated by the white arrows) and astrocytic endfeet making contact is absent (bottom panel). Visual inspection of astrocytes indicates there was no obvious astrocytic activation at 24 h after LPS. Similar effects were seen in the parietal cortex and thalamus (data not shown).

4. Discussion

The results show a relatively rapid activation of most of the microglia in both the hippocampus and the parietal cortex starting 6–12 h after LPS exposure. Within 24 h, the microglia were fully activated and more closely associated with the brain vasculature but not the neurons in the hippocampus, parietal cortex and thalamus. The positioning of these microglia were very similar to that previously described for perivascular microglia (Graeber and Streit, 1990). The microglial activation at 72 h was only slightly less than that seen at 24 h. At none of the time points evaluated did we see evidence of macrophages adhering to vasculature or inside the BBB. As well, Ki67 labeling indicated almost no newborn cells within the cortex or hippocampus, indicating that microglia are not proliferating due to this acute LPS exposure (data not shown). The microglial activation was still apparently present at a slightly lower level at 2 weeks but additional research is necessary to validate this longer-term effect. This time course of activation is similar to that previously observed with LPS *in vivo* in mouse (Madore et al., 2013) and in humans (Sandiego et al., 2015).

We observed that these events occurred in the absence of neurodegeneration as detected by FJc. The lack of astrogliosis also is consistent with a lack of neurodegeneration. In some instances, the

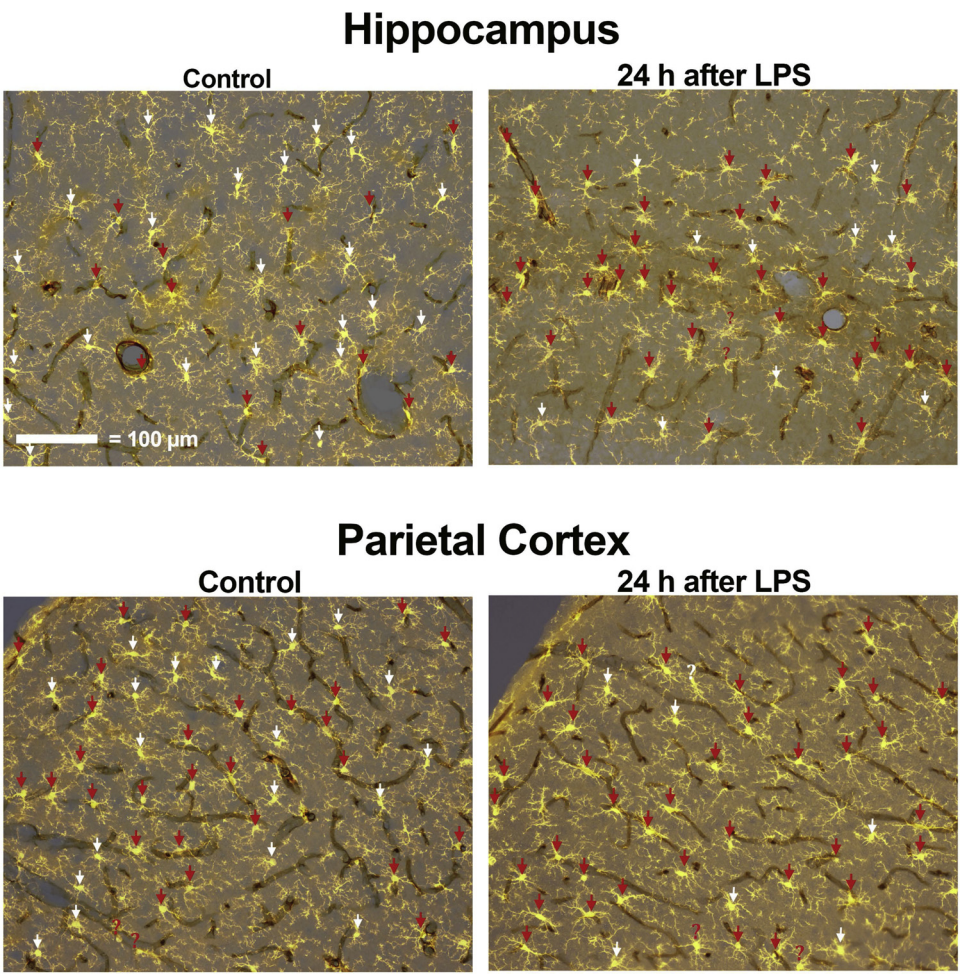

Fig. 4. An alternate means of visualization of distances of microglia soma to the closest blood vessel after LPS. The images shown in this figure were from the types of images seen in Fig. 3 but altered to make it easier for the viewer to observe the differences in distances. The red arrows indicate microglia soma that are < 3 µm from the closest vessel white arrows identify those further away. These types of images for five control and six24 h after LPS were generated in the hippocampus (Supplemental Fig. 7) parietal cortex (Supplemental Figure 8) and thalamus (Supplemental Figure 9) for the readers' viewing. Magnification was the same for all four panels and the magnification bar is shown in the lower left of the upper left panel. (For interpretation of the references to colour in this figure legend, the reader is referred to the web version of this article).

microglial soma or large proximal processes appear to come into direct contact with vasculature where astrocytic endfeet are no longer present. There was clear evidence that the microglia in the hippocampus are migrating closer (apparent average distance decreased about 58 %) to the vasculature (within 1 µm) 24 h after LPS exposure. These migrations were somewhat less in the thalamus (28 %) and not prominent in the parietal cortex. However, under control conditions the average distance in the cortex (about 4 µm) was 42 % that seen in the thalamus and 63 % that seen in the hippocampus. There would likely be a limit to the distance of the microglial soma to the vasculature in many cases since most (well over 95 %) of the astrocytic endfeet are still intact after LPS. It is not clear to what degree the astrocytic end feet and their processes that connect them to the astrocytic soma inhibit the migration of the microglia soma and processes towards vasculature. The end feet substantially, but not completely, cover much of the abluminal surface area of smaller vasculature/ capillaries (Abbott et al., 2006). Thus, they may pose some limitations on microglial soma towards the smaller vasculature. It should be noted that this distance calculations were determined in two dimensions and may slightly underestimate the precise three-dimensional distance. Over all brain regions there was a significant tendency for an increase in the number of microglia to be < 1 µm from the closest vessel, and total microglial soma area within 1 µm of the closest vessel significantly increased in all three regions. This is likely due to the increase in soma size within 1 µm of the closest vessel after LPS, and in some cases the elongation of microglia soma within 1 µm to the vasculature.

These observations for microglial actions are consistent with a response to LPS in relation to: 1) binding to microglia processes residing on vasculature; and 2) possibly damaging vasculature and/or astrocyte endfeet and causing the release of cytokines. A schematic of the possible ways that LPS may interact with the vasculature is shown in Fig. 7. One of the most likely mechanisms is an LPS interaction with microglia processes in contact with vasculature. LPS can bind to both Cd14 and Tlr4 receptors on microglia and result in their activation *in vivo* as well as *in vitro* (Cao et al., 2009; Doring et al., 2017; Harry, 2013; Janova et al., 2016; Lehnardt et al., 2002; Parajuli et al., 2012). Since the primary source of the LPS in brain would be from the circulating blood through the vasculature, it follows that the microglia likely would ultimately be drawn to the vasculature through chemotaxis-like response.

Another possibility is that LPS directly affects the integrity of cerebral vascular endothelial cells and/or their tight junctions (Banks et al., 2015; Boitsova et al., 2018; Martin et al., 2018; Sumbria et al., 2018). We did not detect any leakage of IgG or albumin into the brain at either 3 h or 6 h post LPS. However, this method would only detect larger disruptions of vasculature. Also, we have previously observed that the METH-induced damage to the BBB allowing IgG entry into the brain of rats and mice is transient, and often lasts less than 2 h in some cases (Bowyer and Hanig, 2014). Thus, if LPS acts like METH, causing transient leakage of the BBB, it possible that we would not have collected tissue at the optimal time point to detect this event. We cannot rule out the possibility that there was some BBB leakage due to LPS.

If vascular damage is occurring, one would expect cytokines to be released by the vascular endothelium. We have previously postulated that this may be occurring with vascular-directed microglial responses due to damage to the vasculature resulting from neurotoxic METH exposures. The proposed cytokines in particular are Ccl2, Ccl7, and Ccl20 (Bowyer et al., 2017). These cytokines have 5-fold or greater mRNA expression in all brain regions including meninges and associated

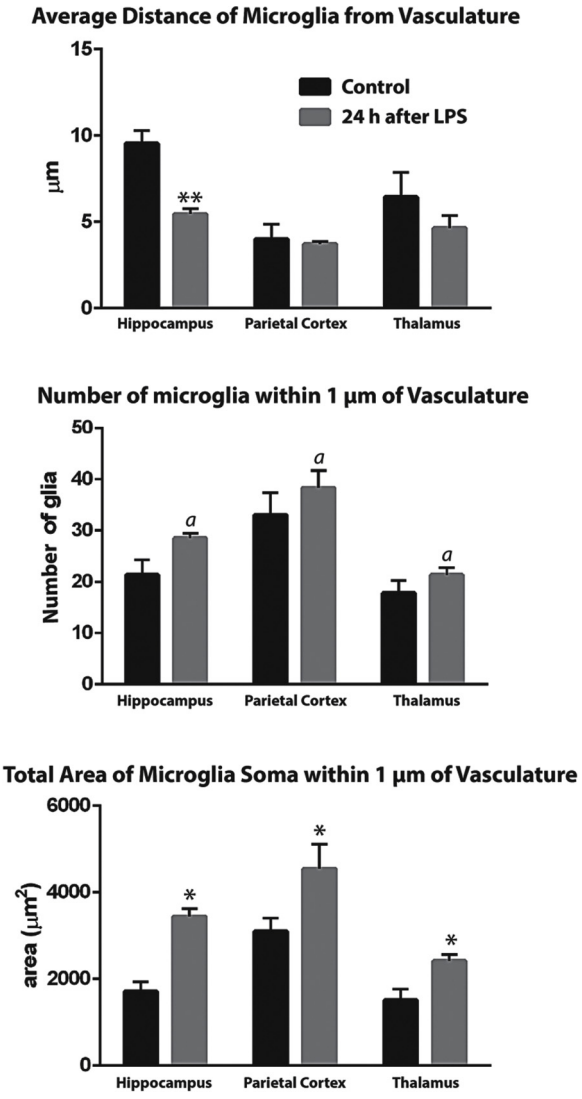

Fig. 5. Spatial relationships between microglia and vasculature in the hippocampus, parietal cortex, and thalamus with respect to size and distance. The original micrographs (overlays shown in Fig. 3 for hippocampus and thalamus) were used for determining the spatial relationships between the microglia and vasculature. The top bar graph shows the effect of LPS on the average distance of the microglia to the closest vessel. Two-way ANOVA with Sidak's post hoc showed that there was significant effect for both region ($P \leq 0.001$) and treatment ($P \leq 0.01$) on the average distance between microglia and the closest vessel. LPS significantly decreased this distance in the hippocampus ($P \leq 0.05$) but did not reach significance in the parietal cortex or thalamus. The number of microglia appearing within 1 μm of the closest vessel are shown for control and after LPS in the middle bar graph. There was a trend, although insignificant, towards an increase in the numbers after LPS in all regions using a two-way ANOVA. In the bottom bar graph the total area of microglia soma within 1 μm of the closest vessel was significantly increased all regions (multiple t-tests with false discovery rate of 6 %). * Significantly different from control at $P \leq 0.05$. [a] The number of microglia across all regions were likely to be less than 1 μm from the closest vessel after LPS at $P \leq 0.05$.

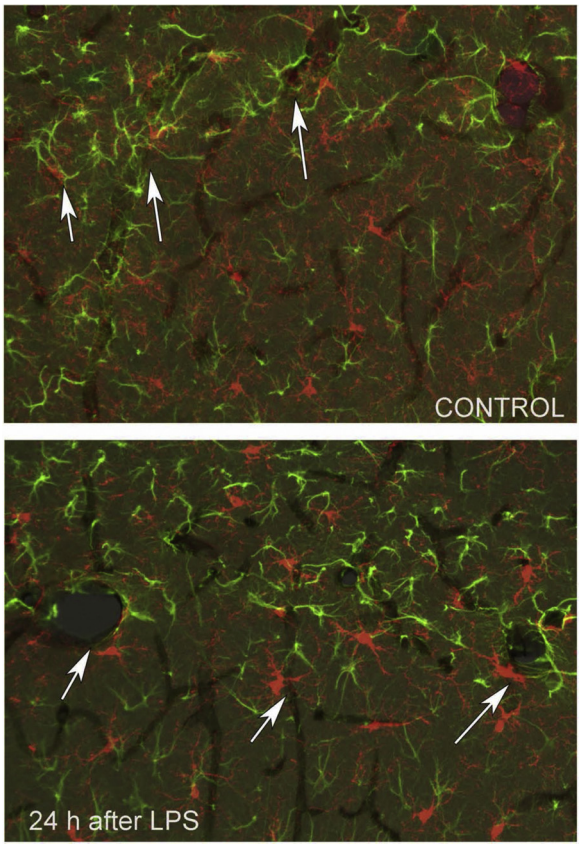

Fig. 6. The relative distribution of astrocytes, microglia and vasculature in hippocampus 24 h after LPS. Cd31-DAB immunolabeled vasculature (brown), Iba1-Cy5 immunolabeled microglia (red) and GFAP-FITC immunolabeled astrocytes (green) are shown in control (upper panel) and 24 h after LPS (lower panel). The microglia have greatly increased in size and are now juxtaposed to the vasculature 24 h after LPS exposure. In the top panel the white arrows indicate just some of the astrocytic contacts with the vasculature in the control. There are only few examples of microglia making prominent contact with vasculature in the control but in the LPS treated animals there are many examples of this as indicated by the white arrows. As well, in these regions it appears that the astrocytic contacts with the vasculature have been lost. Magnification is shown in the top left panel. (For interpretation of the references to colour in this figure legend, the reader is referred to the web version of this article).

vasculature and choroid plexus after either neurotoxic METH or amphetamine exposures (Bowyer et al., 2013; Kelly et al., 2012). However, single cell mRNA expression of vascular endothelium is necessary to determine if endothelium is the source of these three cytokines. An additional observation implicating the vasculature in the observed effects of LPS is the widespread distribution of the response in the brain. Neurotoxic responses to neural damage, including neuroinflammatory responses, characteristically are region and cell-type specific (O'Callaghan et al., 2014). In contrast, neuroinflammatory responses to LPS, such as those observed here and in a previous study with LPS (Kelly et al., 2018), are brain-wide. A brain-wide pattern of effect is consistent with a vascular target. In several previous studies by O'Callaghan and colleagues, corticosterone-induced stress has been shown to significantly exacerbate the neuroimmune response by METH (Kelly et al., 2012) and a mouse model of Gulf War Illness (Koo et al., 2018; Locker et al., 2017; O'Callaghan et al., 2015). Corticosterone, as a stressor mimic, also exacerbates both the neurotoxicity (neurodegeneration) and the neuroimmune response to METH, and some of this microglial activation resulting from METH toxicity is vascular directed (Bowyer et al., 2017).

We observed, qualitatively, an apparent loss in astrocytic contact with vasculature with a concomitant increase in microglial juxtaposed to the vasculature at 24 h after LPS. This may be the result of either vascular or astrocyte damage resulting from LPS. In such a case, it would be easy to envision astrocytes as a source of cytokine release due to LPS. Furthermore, in primary cultures of human or mouse astrocytes, LPS has been shown to directly affect astrocytic activation "status" and enhance cytokine expression (Hinojosa et al., 2013; Semple et al., 2010; Tarassishin et al., 2014). However, it is not clear how the microglia

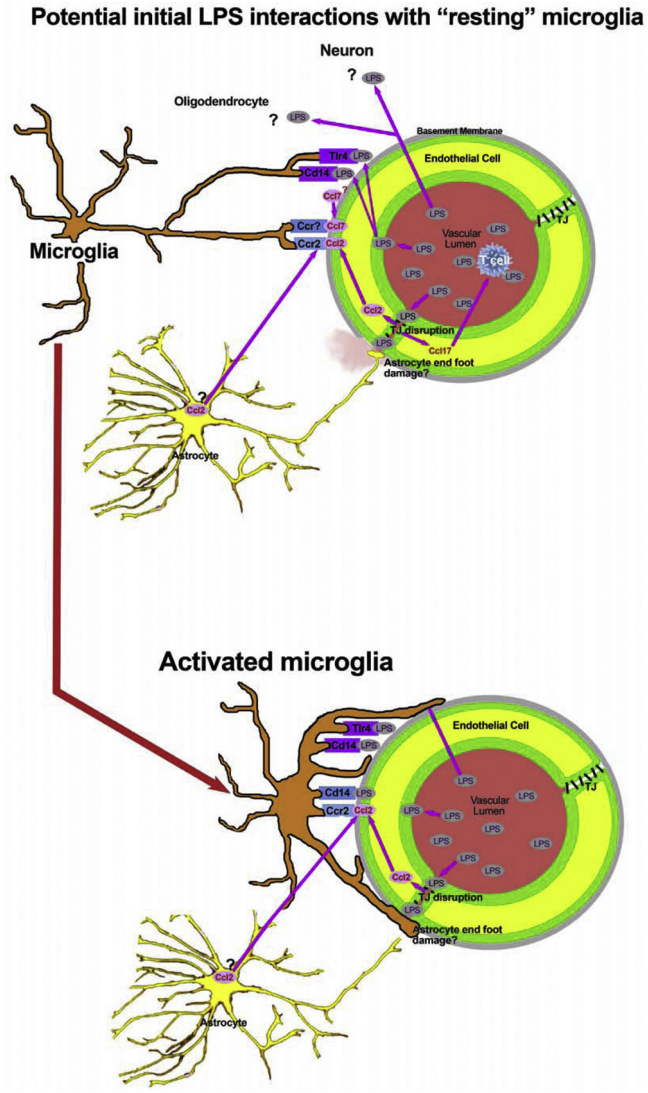

Fig. 7. Schematic of putative mechanisms by which vascular-directed microglial activation might result from LPS exposure. The abbreviations are: Ccl2, C-C motif chemokine ligand 2; Ccl17, C-C motif chemokine ligand 17; Ccr2, C-C motif chemokine receptor 2; Cd14, cluster of differentiation 14; LPS, lipopolysaccharides; Tlr4, toll-like receptor 4. The cell in the middle of the vascular lumen represents the T-cells in circulating blood that can respond to Ccl17.

might direct their responses to the vasculature if they receive Ccl2 cytokine signals from astrocytes, unless it was from their displaced endfeet. Finally, we did not characterize the activation of microglia that occurs in white matter where oligodendrocytes prevail. However, from a subjective standpoint such microglial activation did take place in our study. This could be due to either vascular effects or LPS toxicity directly to the oligodendrocytes (Lehnardt et al., 2002).

No matter which one(s) of the previously proposed mechanisms may be responsible for causing the microglia to surround vasculature, such a response may well be an adaptive protective response. LPS released from bacteria would be a signal indicative of an infection and the likelihood that elevated levels of bacteria are circulating in the blood. Thus, the microglia surrounding the vasculature would be in position to intercept or physically block the pathogens from passing through any breaches in the vascular endothelium. It is not clear whether such protective effects occur at a higher dose of 4 mg/ kg LPS, which has been reported to produce neurodegeneration (Qin et al., 2007).

5. Conclusions

We hypothesize that LPS activation results in vascular-direct microglial responses through several mechanisms; 1) binding to Cd14 and Tlr4 receptors on microglia processes residing on vasculature; 2) damaging vasculature which causes them to release of cytokines; 3) and possibly damaging astrocyte endfeet resulting in astrocytic release of cytokine(s). This series of events may be an adaptive response to protect against infection, where the microglia protectively surround the vasculature to prevent pathogen(s) circulating in blood from entering the brain. We have seen this third type of mechanism, where microglia activation results in their subsequent close association with vasculature, with METH-induced and thiamine deficiency neuroinflammation. We proffer that in these responses the vascular-directed microglial activation are a means of protecting against vascular leakage and possibly implicate a vascular repair mechanism. Also, diverting microglial activity away from neuronal interactions (e.g. synaptic integrity and formation) towards the vasculature could be responsible for some of the adverse neurological effects of LPS. Overall, our observations implicate CNS vasculature as an overlooked target of LPS and other inflammogens with respect to playing a direct role in the activation of microglia

Funding

This research was funded by protocol E07579.01 awarded to J.F. Bowyer by the United States Food and Drug Administration.

Credit author statement

John F. Bowyer – Lead author, primary input on experiment design, performed animal dosing and sacrifice, tissue processing and immune-labeling of histological sections, data collection and interpretation of photomicrographs and editing of manuscript.

Sumit Sarkar – Corresponding author, significant input on experimental design, immunolabeling of histological sections, data collection and interpretation of photomicrographs and editing of manuscript.

Susan M. Burks – Significant input involved in writing revisions and generating figures for the manuscript, developed methods for data analysis to determine distances between vasculature and microglia in the histological sections, additional data collection and interpretation of photomicrographs and editing of manuscript.

Jade N. Hess – Some input on writing, tissue processing and immune-labeling of histological sections, data collection and interpretation of photomicrographs and editing of manuscript.

Serena Tolani - Some input on writing, tissue processing and immune-labeling of histological sections, data collection and interpretation of photomicrographs and editing of manuscript.

James P. O'Callaghan – Extensive input on experiment design, significant input as an author, interpretation experimental results editing of manuscript

Joseph P. Hanig – Significant input on experiment design, significant input as an author, interpretation experimental results and editing of manuscript.

Disclaimer

The authors are solely employed by the U.S. government and are not affiliated or employed with any company or have any financial interests relating the research presented or its implications.

This manuscript has been processed for clearing/ consent for publication via the FDA document tracking system. However, the contents of this manuscript do not necessarily reflect the views and policies of the U.S. Food and Drug Administration, nor does the mention of trade names or commercial products constitute endorsement or a recommendation for use.

Declaration of Competing Interest

The authors declare that they have no known competing financial interests or personal relationships that could have appeared to influence the work reported in this paper.

Acknowledgements

The authors would like to thank Bonnie Robinson and James Raymick for their assistance in animal dosing and sacrifice. We would like to thank Dr. Brian Mikeworth for his assistance with our efforts to characterize size changes in microglia during activation.

Appendix A. Supplementary data

Supplementary material related to this article can be found, in the online version, at doi:https://doi.org/10.1016/j.neuro.2020.01.014.

References

Abbott, N.J., Ronnback, L., Hansson, E., 2006. Astrocyte-endothelial interactions at the blood-brain barrier. Nat. Rev. Neurosci. 7, 41–53.
Aldskogius, H., Liu, L., Svensson, M., 1999. Glial responses to synaptic damage and plasticity. J. Neurosci. Res. 58, 33–41.
Banks, W.A., Gray, A.M., Erickson, M.A., Salameh, T.S., Damodarasamy, M., Sheibani, N., Meabon, J.S., Wing, E.E., Morofuji, Y., Cook, D.G., Reed, M.J., 2015. Lipopolysaccharide-induced blood-brain barrier disruption: roles of cyclooxygenase, oxidative stress, neuroinflammation, and elements of the neurovascular unit. J. Neuroinflammation 12, 223.
Bisht, K., Sharma, K., Tremblay, M.E., 2018. Chronic stress as a risk factor for Alzheimer's disease: roles of microglia-mediated synaptic remodeling, inflammation, and oxidative stress. Neurobiol. Stress 9, 9–21.
Boitsova, E.B., Morgun, A.V., Osipova, E.D., Pozhilenkova, E.A., Martinova, G.P., Frolova, O.V., Olovannikova, R.Y., Tohidpour, A., Gorina, Y.V., Panina, Y.A., Salmina, A.B., 2018. The inhibitory effect of LPS on the expression of GPR81 lactate receptor in blood-brain barrier model in vitro. J. Neuroinflammation 15, 196.
Bowyer, J.F.H., Hanig, J.P., 2014. Amphetamine- and methamphetamine-induced hyperthermia: implications of the effects produced in brain vasculature and peripheral organs to forebrain neurotoxicity. Temperature 1, 172–182.
Bowyer, J.F., Peterson, S.L., Rountree, R.L., Tor-Agbidye, J., Wang, G.J., 1998. Neuronal degeneration in rat forebrain resulting from D-amphetamine-induced convulsions is dependent on seizure severity and age. Brain Res. 809, 77–90.
Bowyer, J.F., Patterson, T.A., Saini, U.T., Hanig, J.P., Thomas, M., Camacho, L., George, N.I., Chen, J.J., 2013. Comparison of the global gene expression of choroid plexus and meninges and associated vasculature under control conditions and after pronounced hyperthermia or amphetamine toxicity. BMC Genomics 14, 147.
Bowyer, J.F., Sarkar, S., Tranter, K.M., Hanig, J.P., Miller, D.B., O'Callaghan, J.P., 2016. Vascular-directed responses of microglia produced by methamphetamine exposure: indirect evidence that microglia are involved in vascular repair? J. Neuroinflammation 13, 64.
Bowyer, J.F., Tranter, K.M., Sarkar, S., George, N.I., Hanig, J.P., Kelly, K.A., Michalovicz, L.T., Miller, D.B., O'Callaghan, J.P., 2017. Corticosterone and exogenous glucose alter blood glucose levels, neurotoxicity, and vascular toxicity produced by methamphetamine. J. Neurochem.
Bowyer, J.F., Tranter, K.M., Robinson, B.L., Hanig, J.P., Faubion, M.G., Sarkar, S., 2018a. The time course of blood brain barrier leakage and its implications on the progression of methamphetamine-induced seizures. Neurotoxicology 69, 130–140.
Bowyer, J.F., Tranter, K.M., Sarkar, S., Hanig, J.P., 2018b. Microglial activation and vascular responses that are associated with early thalamic neurodegeneration resulting from thiamine deficiency. Neurotoxicology 65, 98–110.
Bruce-Keller, A.J., 1999. Microglial-neuronal interactions in synaptic damage and recovery. J. Neurosci. Res. 58, 191–201.
Buchanan, J.B., Sparkman, N.L., Johnson, R.W., 2010. Methamphetamine sensitization attenuates the febrile and neuroinflammatory response to a subsequent peripheral immune stimulus. Brain Behav. Immun. 24, 502–511.
Cao, L., Tanga, F.Y., Deleo, J.A., 2009. The contributing role of CD14 in toll-like receptor 4 dependent neuropathic pain. Neuroscience 158, 896–903.
Catorce, M.N., Gevorkian, G., 2016. LPS-induced murine neuroinflammation model: main features and suitability for pre-clinical assessment of nutraceuticals. Curr. Neuropharmacol. 14, 155–164.
Dantzer, R., O'Connor, J.C., Freund, G.G., Johnson, R.W., Kelley, K.W., 2008. From inflammation to sickness and depression: when the immune system subjugates the brain. Nat. Rev. Neurosci. 9, 46–56.
Doring, C., Regen, T., Gertig, U., van Rossum, D., Winkler, A., Saiepour, N., Bruck, W., Hanisch, U.K., Janova, H., 2017. A presumed antagonistic LPS identifies distinct functional organization of TLR4 in mouse microglia. Glia 65, 1176–1185.
Graeber, M.B., 2010. Changing face of microglia. Science 330, 783–788.
Graeber, M.B., Streit, W.J., 1990. Perivascular microglia defined. Trends Neurosci. 13, 366.
Graeber, M.B., Streit, W.J., 2010. Microglia: biology and pathology. Acta Neuropathol. 119, 89–105.
Guerville, M., Boudry, G., 2016. Gastrointestinal and hepatic mechanisms limiting entry and dissemination of lipopolysaccharide into the systemic circulation. Am. J. Physiol. Gastrointest. Liver Physiol. 311, G1–G15.
Harry, G.J., 2013. Microglia during development and aging. Pharmacol. Ther. 139, 313–326.
Hinojosa, A.E., Caso, J.R., Garcia-Bueno, B., Leza, J.C., Madrigal, J.L., 2013. Dual effects of noradrenaline on astroglial production of chemokines and pro-inflammatory mediators. J. Neuroinflammation 10, 81.
Hoogland, I.C., Houbolt, C., van Westerloo, D.J., van Gool, W.A., van de Beek, D., 2015. Systemic inflammation and microglial activation: systematic review of animal experiments. J. Neuroinflammation 12, 114.
Imai, Y., Ibata, I., Ito, D., Ohsawa, K., Kohsaka, S., 1996. A novel gene iba1 in the major histocompatibility complex class III region encoding an EF hand protein expressed in a monocytic lineage. Biochem. Biophys. Res. Commun. 224, 855–862.
Ito, D., Imai, Y., Ohsawa, K., Nakajima, K., Fukuuchi, Y., Kohsaka, S., 1998. Microglia-specific localisation of a novel calcium binding protein, Iba1. Brain Res. Mol. Brain Res. 57, 1–9.
Janova, H., Bottcher, C., Holtman, I.R., Regen, T., van Rossum, D., Gotz, A., Ernst, A.S., Fritsche, C., Gertig, U., Saiepour, N., Gronke, K., Wrzos, C., Ribes, S., Rolfes, S., Weinstein, J., Ehrenreich, H., Pukrop, T., Kopatz, J., Stadelmann, C., Salinas-Riester, G., Weber, M.S., Prinz, M., Bruck, W., Eggen, B.J., Boddeke, H.W., Priller, J., Hanisch, U.K., 2016. CD14 is a key organizer of microglial responses to CNS infection and injury. Glia 64, 635–649.
Kasa, A., Csortos, C., Verin, A.D., 2015. Cytoskeletal mechanisms regulating vascular endothelial barrier function in response to acute lung injury. Tissue Barriers 3, e974448.
Kelly, K.A., Miller, D.B., Bowyer, J.F., O'Callaghan, J.P., 2012. Chronic exposure to corticosterone enhances the neuroinflammatory and neurotoxic responses to methamphetamine. J. Neurochem.
Kelly, K.A., Michalovicz, L.T., Miller, J.V., Castranova, V., Miller, D.B., O'Callaghan, J.P., 2018. Prior exposure to corticosterone markedly enhances and prolongs the neuroinflammatory response to systemic challenge with LPS. PLoS One 13, e0190546.
Khakpour, S., Wilhelmsen, K., Hellman, J., 2015. Vascular endothelial cell Toll-like receptor pathways in sepsis. Innate Immun. 21, 827–846.
Koo, B.B., Michalovicz, L.T., Calderazzo, S., Kelly, K.A., Sullivan, K., Killiany, R.J., O'Callaghan, J.P., 2018. Corticosterone potentiates DFP-induced neuroinflammation and affects high-order diffusion imaging in a rat model of Gulf War Illness. Brain Behav. Immun. 67, 42–46.
Kraft, A.D., Harry, G.J., 2011. Features of microglia and neuroinflammation relevant to environmental exposure and neurotoxicity. Int. J. Environ. Res. Public Health 8, 2980–3018.
Laflamme, N., Soucy, G., Rivest, S., 2001. Circulating cell wall components derived from gram-negative, not gram-positive, bacteria cause a profound induction of the gene-encoding Toll-like receptor 2 in the CNS. J. Neurochem. 79, 648–657.
Lehnardt, S., Lachance, C., Patrizi, S., Lefebvre, S., Follett, P.L., Jensen, F.E., Rosenberg, P.A., Volpe, J.J., Vartanian, T., 2002. The toll-like receptor TLR4 is necessary for lipopolysaccharide-induced oligodendrocyte injury in the CNS. J. Neurosci. 22, 2478–2486.
Lenz, K.M., Nelson, L.H., 2018. Microglia and beyond: innate immune cells As regulators of brain development and behavioral function. Front. Immunol. 9, 698.
Locker, A.R., Michalovicz, L.T., Kelly, K.A., Miller, J.V., Miller, D.B., O'Callaghan, J.P., 2017. Corticosterone primes the neuroinflammatory response to Gulf War Illness-relevant organophosphates independently of acetylcholinesterase inhibition. J. Neurochem. 142, 444–455.
Lopes, P.C., 2016. LPS and neuroinflammation: a matter of timing. Inflammopharmacology 24, 291–293.
Madore, C., Joffre, C., Delpech, J.C., De Smedt-Peyrusse, V., Aubert, A., Coste, L., Laye, S., Nadjar, A., 2013. Early morphofunctional plasticity of microglia in response to acute lipopolysaccharide. Brain Behav. Immun. 34, 151–158.
Martin, C.R., Osadchiy, V., Kalani, A., Mayer, E.A., 2018. The brain-gut-microbiome axis. Cell. Mol. Gastroenterol. Hepatol. 6, 133–148.
O'Callaghan, J.P., Sriram, K., Miller, D.B., 2008. Defining "neuroinflammation". Ann. N. Y. Acad. Sci. 1139, 318–330.
O'Callaghan, J.P., Kelly, K.A., VanGilder, R.L., Sofroniew, M.V., Miller, D.B., 2014. Early activation of STAT3 regulates reactive astrogliosis induced by diverse forms of neurotoxicity. PLoS One 9, e102003.
O'Callaghan, J.P., Kelly, K.A., Locker, A.R., Miller, D.B., Lasley, S.M., 2015. Corticosterone primes the neuroinflammatory response to DFP in mice: potential animal model of Gulf War Illness. J. Neurochem. 133, 708–721.
On, N.H., Savant, S., Toews, M., Miller, D.W., 2013. Rapid and reversible enhancement of blood-brain barrier permeability using lysophosphatidic acid. J. Cereb. Blood Flow Metab. 33, 1944–1954.
Parajuli, B., Sonobe, Y., Kawanokuchi, J., Doi, Y., Noda, M., Takeuchi, H., Mizuno, T., Suzumura, A., 2012. GM-CSF increases LPS-induced production of proinflammatory mediators via upregulation of TLR4 and CD14 in murine microglia. J. Neuroinflammation 9, 268.
Qin, L., Wu, X., Block, M.L., Liu, Y., Breese, G.R., Hong, J.S., Knapp, D.J., Crews, F.T., 2007. Systemic LPS causes chronic neuroinflammation and progressive neurodegeneration. Glia 55, 453–462.
Rosadini, C.V., Kagan, J.C., 2017. Early innate immune responses to bacterial LPS. Curr. Opin. Immunol. 44, 14–19.
Sandiego, C.M., Gallezot, J.D., Pittman, B., Nabulsi, N., Lim, K., Lin, S.F., Matuskey, D., Lee, J.Y., O'Connor, K.C., Huang, Y., Carson, R.E., Hannestad, J., Cosgrove, K.P., 2015. Imaging robust microglial activation after lipopolysaccharide administration in humans with PET. Proc. Natl. Acad. Sci. U. S. A. 112, 12468–12473.

Savage, J.C., Picard, K., Gonzalez-Ibanez, F., Tremblay, M.E., 2018. A brief history of microglial ultrastructure: distinctive features, phenotypes, and functions discovered over the past 60 years by Electron microscopy. Front. Immunol. 9, 803.
Schmued, L.C., Stowers, C.C., Scallet, A.C., Xu, L., 2005. Fluoro-Jade C results in ultra high resolution and contrast labeling of degenerating neurons. Brain Res. 1035, 24–31.
Semple, B.D., Frugier, T., Morganti-Kossmann, M.C., 2010. CCL2 modulates cytokine production in cultured mouse astrocytes. J. Neuroinflammation 7, 67.
Sholl, D.A., 1956. The measurable parameters of the cerebral cortex and their significance in its organization. Prog. Neurobiol. 324–333.
Streit, W.J., 2010. Microglial activation and neuroinflammation in Alzheimer's disease: a critical examination of recent history. Front. Aging Neurosci. 2, 22.
Sumbria, R.K., Grigoryan, M.M., Vasilevko, V., Paganini-Hill, A., Kilday, K., Kim, R., Cribbs, D.H., Fisher, M.J., 2018. Aging exacerbates development of cerebral microbleeds in a mouse model. J. Neuroinflammation 15, 69.
Tarassishin, L., Suh, H.S., Lee, S.C., 2014. LPS and IL-1 differentially activate mouse and human astrocytes: role of CD14. Glia 62, 999–1013.
Tremblay, M.E., 2011. The role of microglia at synapses in the healthy CNS: novel insights from recent imaging studies. Neuron Glia Biol. 7, 67–76.
Xaio, H., Banks, W.A., Niehoff, M.L., Morley, J.E., 2001. Effect of LPS on the permeability of the blood-brain barrier to insulin. Brain Res. 896, 36–42.